Native Defects and their Doping Response in the Lithium Solid Electrolyte $Li_7La_3Zr_2O_{12}$

Alexander G. Squires,[1,2] David O. Scanlon,[3,4,2,5] and Benjamin J. Morgan[1,2,*]

[1] *Department of Chemistry, University of Bath, Bath, BA2 7AX.*
[2] *The Faraday Institution, Quad One, Harwell Science and Innovation Campus, Didcot, UK.*
[3] *Department of Chemistry, University College London, 20 Gordon Street, London, WC1H 0AJ.*
[4] *Diamond Light Source Ltd., Diamond House, Harwell Science and Innovation Campus, Didcot, Oxfordshire OX11 0DE, United Kingdom.*
[5] *Thomas Young Centre, University College London, Gower Street, London WC1E 6BT, UK*

S1. COMPARISON OF HSE06, PBESOL+U, AND PBESOL FUNCTIONALS FOR THE $V_{Li}^{\times}$ DEFECT

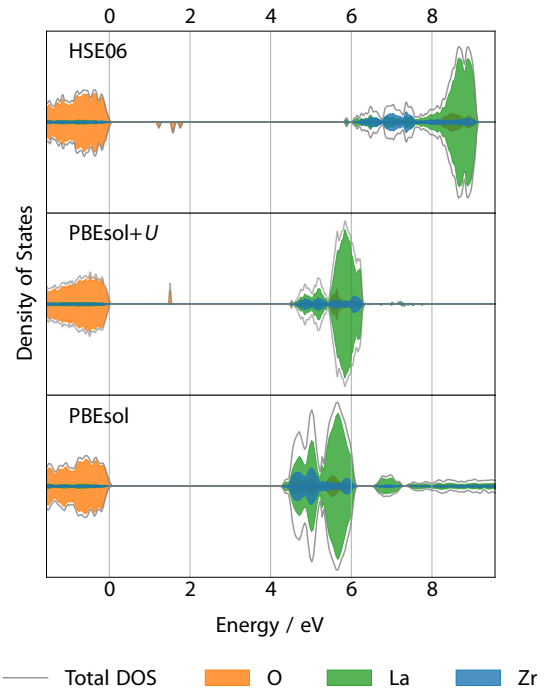

FIG. S1. Density of state plots for the $V_{Li}^{\times}$ using as-labelled exchange-correlation functionals. *Source:* The data and code used to generate this figure, and the figure file, are available under the MIT license as part of Ref. 1.

When modelling defects, it is desirable for both the band gap of the stoichiometric system, and the energies of different defect charge states, to be accurate.[2] In this work we have used the HSE06 hybrid functional, which is expected to give more accurate results relative to standard, cheaper, LDA or GGA functionals, for both the band gap and defect formation eneriges. To illustrate the advantages of using a hybrid functional, such as HSE06, here we show the calculated densities of states for the $V_{Li}^{\times}$ defect as predicted using HSE06,[3] PBEsol with a "+U" on-site Hubbard correction,[4] and standard PBEsol[5] (Fig. S1). HSE06 predicts a band gap of 5.9 eV, which is close to experimental values of $\sim$ 6.0 eV.[6] The neutral $V_{Li}^{\times}$ introduces an excess hole. In wide gap oxides, holes are typically expected to localise on oxygen $2p$ orbitals as small polarons,[7] and this is indeed the behaviour obtained with HSE06, which predicts an empty defect state $\sim$ 1.5 eV above the valence-band maximum, corresponding to a localised oxygen 2p state (Fig. S2a)). Using PBEsol+U, with $U(O_p)$=6.7 eV,[8] again we obtain a localised oxygen 2p hole-state in the gap (Fig. S2b)). While the +U correction does give an approximate correction to the self-interaction error for these oxygen-hole states, the band gap is underestimated relative to the HSE06 and experimental values. Finally, PBEsol not only underestimates the band gap, but gives a quantitatively incorrect description of the $V_{Li}^{\times}$ defect state: The excess hole now occupies the top of the valence band, and is delocalised over all oxygen atoms in the calculation, corresponding to a "shallow" defect state (Fig. S2c)).

S2. COMPETING PHASES AND STABILITY-REGION ANALYSIS

The region of thermodynamic stability for LLZO was calculated with respect to the following bounding phases: Li, Li_2O, Li_2ZrO_3, Li_6ZrO_7, Li_8ZrO_6, La, La_2O_3, Zr, ZrO_2, and O_2. Details of these calculations can be found in the accompanying dataset (Ref. 9). The competing phases define the stability regions shown in Fig. S3. These stability regions show how, with respect to each metal, stability with respect to oxygen chemical potential appear as narrow strip, with the extrema broadly characterised as metal-rich/oxygen-poor and metal-poor/oxygen-rich environments. Fig. S4 shows these stability regions again, but with the additon of the path taken through the stability region to generate the defect concentrations shown in Fig. 2 in the main manuscript.

S3. INTRINSIC DEFECT CHEMISTRY: DEFECT CONCENTRATIONS VERSUS $\Delta\mu_{Li}$

Fig. S7 shows the change in defect chemistry for a fixed μ_O, as μ_{Li} is varied. The nature of the dominant defects changes much more strongly that under variations in μ_O, as described in the main manuscript.

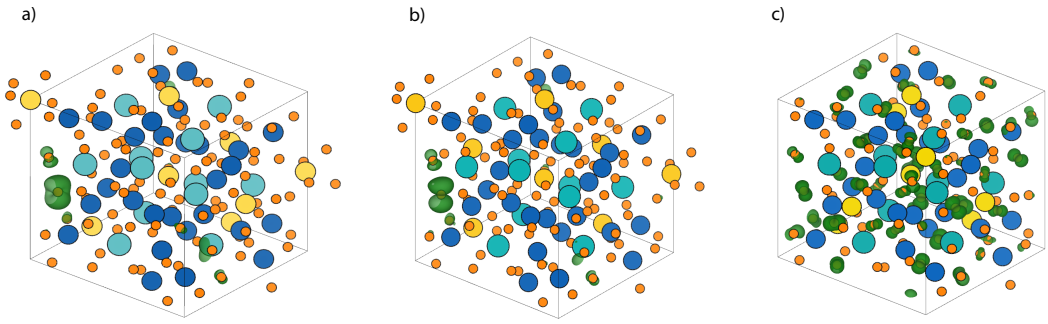

FIG. S2. Partial charge density plots for the excess hole-charge associated with the $V_{\mathrm{Li}}^{\times}$ defect, using (a) HSE06, (b) PBEsol+U and (c) PBEsol. HSE06 and PBEsol+U localise the excess hole–charge-density as a small polaron. PBEsol erroneously delocalises the hole across several oxygen ions. *Source:* The data used to generate this figure are available under the MIT license as part of Ref. 9.

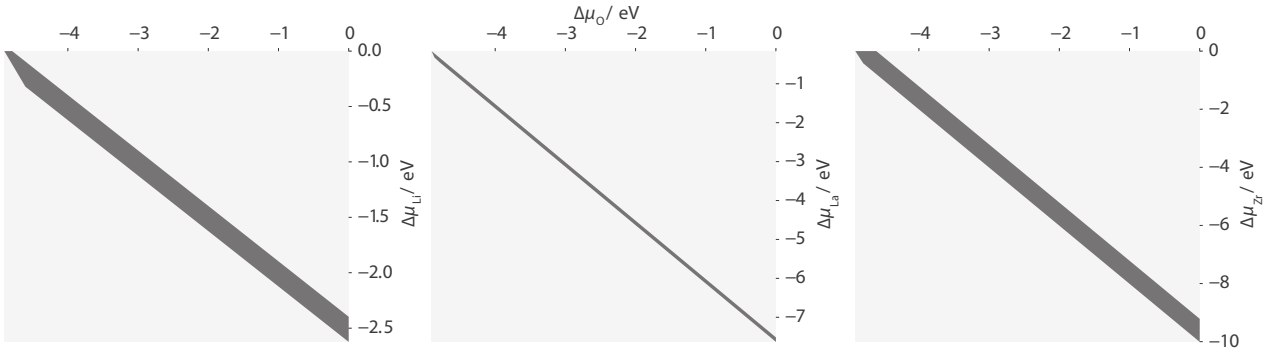

FIG. S3. Chemical potential stability regions with respect to μ_{O} and μ_{metal} for each of Li, La, and Zr. *Source:* The data and code used to generate this figure, and the figure file, are available under the MIT license as part of Ref. 1.

S4. OXYGEN VACANCY MOBILITY CALCULATIONS

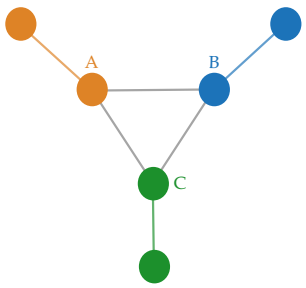

FIG. S5. Network graph of the nearest-neighbour–oxygen conduction network in tetragonal LLZO. The three distinct oxygen sites in the tetragonal phase give six inequivalent nearest-neighbour pathways.

Tetragonal LLZO contains six inequivalent O—O nearest-neighbour pairs.The potential paths in tetragonal LLZO for oxygen migration are shown in Fig. S5. Table S1 contains the diffusion barriers for each path, obtained from climbing-image nudged elastic band calculations (CI-NEB).[10] Each CI-NEB calculation included seven images between the two relevant end-points, and was performed using the PBEsol GGA functional.[5]

Pathway	Energy [eV]
A → A	0.89
A → B	0.78
A → C	0.73
B → B	0.78
B → C	0.77
C → C	1.15

TABLE S1. Oxygen vacancy migration energy barriers determined from CI-NEB calculations.

S5. FULL TRANSITION LEVEL DIAGRAMS FOR SUPERVALENT DOPING UNDER VARIED CHEMICAL POTENTIAL REGIMES

Fig. S6 shows the full transition-level diagrams for all native defects under the two different doping regimes (Li-poor / Zr-rich and Li-rich / Zr-poor) described in the main manuscript.

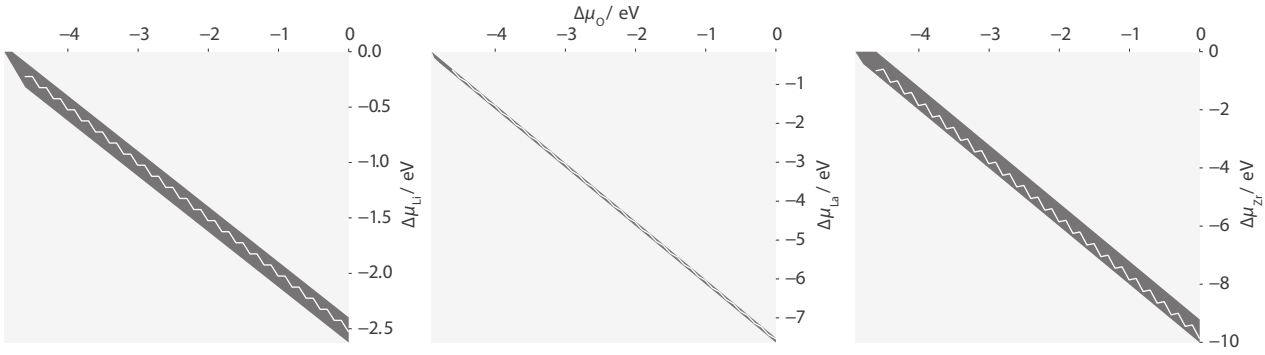

FIG. S4. Chemical potential stability regions with respect to μ_{O} and μ_{metal} for each of Li, La, and Zr plotted showing (in white) the path taken through each stability region to calculate the concentrations through Fig. 2 in the main manuscript. *Source:* The data and code used to generate this figure, and the figure file, are available under the MIT license as part of Ref. 1.

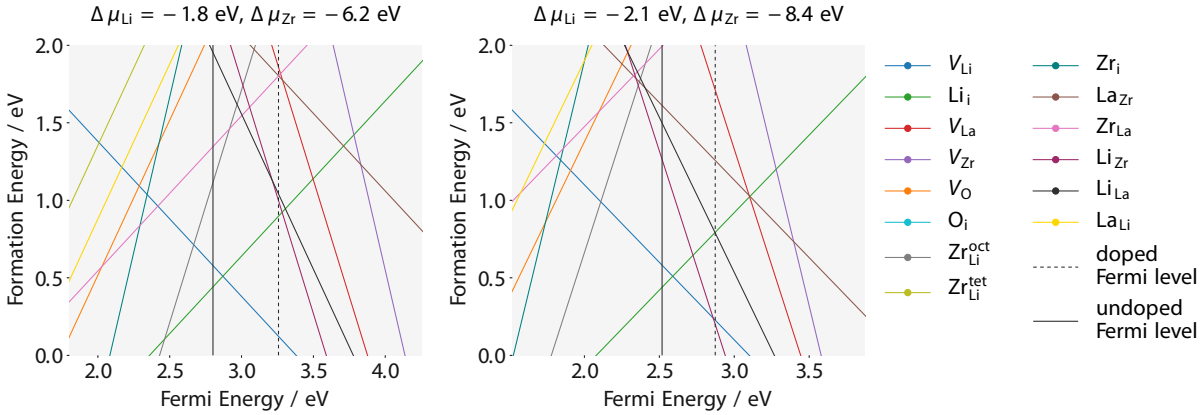

FIG. S6. Defect formation energies as a function of Fermi energy for the given chemical potentials. In each diagram we show the Fermi level position before, and after supervalent doping ($0.15\,M_{\mathrm{Li}}^{\bullet\bullet}$ per formula unit). These plots are equivalent to those shown in Fig. 5 in the main manuscript, but with all defect formation energies shown. *Source:* The data and code used to generate this figure, and the figure file, are available under the MIT license as part of Ref. 1

S6. RELATIONSHIP BETWEEN ZIRCONIUM AND LITHIUM CHEMICAL POTENTIALS

To understand whether a set of chemical potentials that LLZO is formed under will give rise to the simple compensation mechanism suggested by Eqn. 1 in the main manuscript upon doping, we discuss the relationship between the two chemical potentials. The equation of the V'_{Li} line and the $\mathrm{Li}'''_{\mathrm{Zr}}$ line on a transition level diagram (plot of defect formation energy and Fermi energy) are:

$$E_{\mathrm{f}} = E_{\mathrm{f}}^{0}[V'_{\mathrm{Li}}] - E_{\mathrm{F}} \tag{S1}$$

and,

$$E_{\mathrm{f}} = E_{\mathrm{f}}^{0}[\mathrm{Li}'''_{\mathrm{Zr}}] - 3E_{\mathrm{F}} \tag{S2}$$

respectively. E_{f} is the formation energy, E_{F} the Fermi energy, and y-intercept is the formation energy of the defect in the relevant charge state at $E_{\mathrm{F}} = 0$. Assuming equal treatment of corrections and potential alignments, Eqns. S1 and S2 above can be re-written–considering Eqn. 3 in the main manuscript as:

$$E_{\mathrm{F}} = c_{V_{\mathrm{Li}}} + \mu_{\mathrm{Li}} + E_{\mathrm{f}} \tag{S3}$$

and

$$E_{\mathrm{F}} = \frac{c_{\mathrm{Li}_{\mathrm{Zr}}} + \mu_{\mathrm{Li}} + \mu_{\mathrm{Zr}} + E_{\mathrm{f}}}{3} \tag{S4}$$

where c is the concentration of the subscript defect species. The point at which these two lines cross will share the same E_{F}, therefore:

$$3(c_{V_{\mathrm{Li}}} + \mu_{\mathrm{Li}} + E_{\mathrm{f}}) = c_{\mathrm{Li}_{\mathrm{Zr}}} - \mu_{\mathrm{Li}} + \mu_{\mathrm{Zr}} + E_{\mathrm{f}}. \tag{S5}$$

This indicates that the relative balance of chemical potentials for determining whether the formation energy of the $\mathrm{Li}_{\mathrm{Zr}}$ defect will become lower than the formation energy of V_{Li} is $\mu_{\mathrm{Zr}} - 4\mu_{\mathrm{Li}}$. This linear relation only approximately describes the data as for each value of $\mu_{\mathrm{Zr}} - 4\mu_{\mathrm{Li}}$, the chemical potentials of lanthanum and oxygen are bounded, but not fixed.

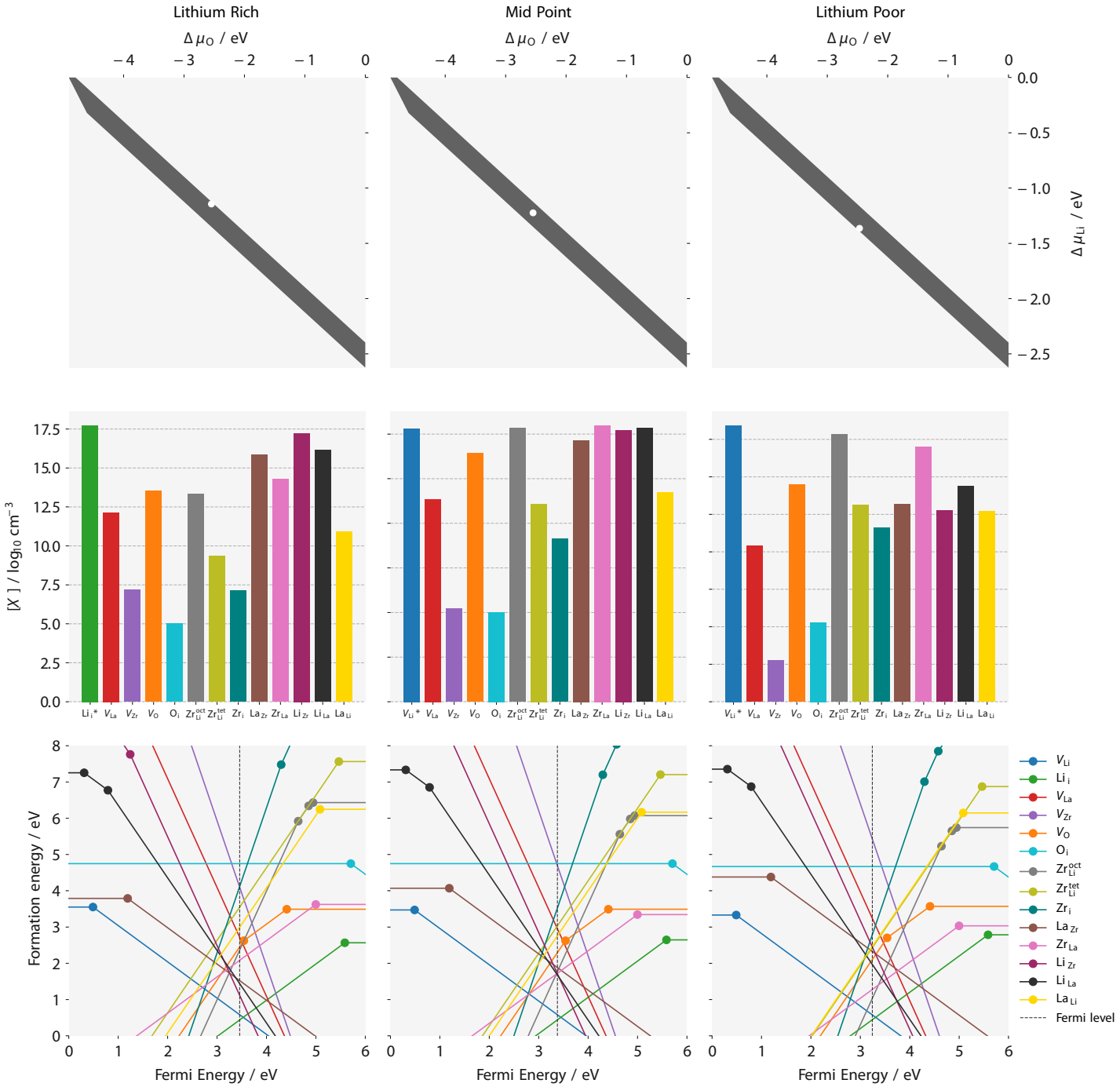

FIG. S7. Equilibrium defect concentrations (middle panels) and defect formation-energies as a function of Fermi energy (bottom panels) at three sets of elemental chemical potentials within the LLZO thermodynamic stability region (top panel). Defect concentrations are calculated at $T = 1500\,\mathrm{K}$. In each case, the bottom panel also shows the corresponding self-consistent Fermi energy (vertical dotted line). *The concentration of lithium vacancies/interstitials is given as a net value, i.e. $[V^*_{\mathrm{Li}}] = [V_{\mathrm{Li}}] - [\mathrm{Li_i}]$. *Source:* The data and code used to generate this figure, and the figure file, are available under the MIT license as part of Ref. 1.

* b.j.morgan@bath.ac.uk

[1] A. G. Squires, D. O. Scanlon, and B. J. Morgan, "GitHub repository containing analysis for "Native Defects and their Doping Response in the Lithium Solid Electrolyte $Li_7La_3Zr_2O_{12}$"." https://github.com/alexsquires/native-defects-in-llzo (accessed 12/18/2019).

[2] S. Lany and A. Zunger, "Assessment of correction methods for the band-gap problem and for finite-size effects in supercell defect calculations: Case studies for ZnO and GaAs," *Phys. Rev. B*, vol. 78, no. 23, pp. 17–20, 2008.

[3] A. V. Krukau, O. A. Vydrov, A. F. Izmaylov, and G. E. Scuseria, "Influence of the exchange screening parameter on the performance of screened hybrid functionals," *J. Chem. Phys.*, vol. 125, no. 22, 2006.

[4] S. L. Dudarev, G. A. Botton, S. Y. Savrasov, C. J. Humphreys, and A. P. Sutton, "Electron-energy-loss spectra and the structural stability of nickel oxide: An lsda+u study," *Phys. Rev. B*, vol. 57, pp. 1505–1509, Jan 1998.

[5] J. Perdew, A. Ruzsinszky, G. Csonka, O. Vydrov, G. Scuseria, L. Constantin, X. Zhou, and K. Burke, "Restoring the Density Gradient-Expansion for Exchange in Solids and Surfaces," *Phys. Rev. Lett.*, vol. 100, no. 13, p. 136406, 2008.

[6] T. Thompson, S. Yu, L. Williams, R. D. Schmidt, R. Garcia-Mendez, J. Wolfenstine, J. L. Allen, E. Kioupakis, D. J. Siegel, and J. Sakamoto, "Electrochemical window of the Li-ion solid electrolyte $Li_7La_3Zr_2O_{12}$," *ACS Energy Lett.*, vol. 2, no. 2, pp. 462–468, 2017.

[7] S. Lany, "Predicting polaronic defect states by means of generalized koopmans density functional calculations," *physica status solidi (b)*, vol. 248, no. 5, pp. 1052–1060, 2011.

[8] The value of $U(O_p)$=6.7 eV was obtained by using the fitting procedure of Lany and Zunger, by selecting a U value that fulfils the generalised Koopmans' condition.[7,11–14]

[9] A. G. Squires, D. O. Scanlon, and B. J. Morgan, "University of Bath data archive containing dataset for "Native Defects and their Doping Response in the Lithium Solid Electrolyte $Li_7La_3Zr_2O_{12}$"." https://researchdata.bath.ac.uk/id/eprint/691 (accessed 12/18/2019).

[10] G. Henkelman, B. P. Uberuaga, and H. Jónsson, "Climbing image nudged elastic band method for finding saddle points and minimum energy paths," *J. Chem. Phys.*, vol. 113, no. 22, pp. 9901–9904, 2000.

[11] S. Lany and A. Zunger, "Polaronic hole localization and multiple hole binding of acceptors in oxide wide-gap semiconductors," *Phys. Rev. B*, vol. 80, p. 085202, 2009.

[12] B. J. Morgan and G. W. Watson, "Polaronic trapping of electrons and holes in anatase TiO_2," *Phys. Rev. B*, vol. 80, no. 233102, p. 233102, 2009.

[13] I. Dabo, A. Ferretti, N. Poilvert, Y. Li, N. Marzari, and M. Cococcioni, "Koopmans' condition for density-functional theory," *Phys. Rev. B*, vol. 82, pp. 1–17, Sept. 2010.

[14] S. Lany and A. Zunger, "Generalized koopmans density functional calculations reveal the deep acceptor state of n-o in zno," *Phys. Rev. B*, vol. 81, no. 20, p. 205209, 2010.